A new diagnostic for tropospheric ozone production

Peter M. Edwards[1]* & Mathew J. Evans[1,2]

[1] Wolfson Atmospheric Chemistry Laboratories, Department of Chemistry, University of York, Heslington, York, YO10 5DD, UK

[2] National Centre for Atmospheric Science, Department of Chemistry, University of York, Heslington, York, YO10 5DD, UK

*pete.edwards@york.ac.uk

Abstract

Tropospheric ozone is important for the Earth's climate and air quality. It is produced during the oxidation of organics in the presence of nitrogen oxides. Due to the range of organic species emitted and the chain like nature of their oxidation, this chemistry is complex and understanding the role of different processes (emission, deposition, chemistry) is difficult. We demonstrate a new methodology for diagnosing ozone production based on the processing of bonds contained within emitted molecules, the fate of which is determined by the conservation of spin of the bonding electrons. Using this methodology to diagnose ozone production in the GEOS-Chem chemical transport model, we demonstrate its advantages over the standard diagnostic. We show that the number of bonds emitted, their chemistry and lifetime, and feedbacks on OH are all important in determining the ozone production within the model and its sensitivity to changes. This insight may allow future model-model comparisons to better identify the root causes of model differences.

1. Introduction

The chemistry of the troposphere is one of oxidation [*Levy*, 1973; *Kroll et al.*, 2011]. Organic compounds together with nitrogen and sulfur containing molecules are emitted into the troposphere where they are oxidised into compounds which can either be: absorbed by the biosphere; are involatile enough to form aerosols; can deposit to the surface; or be taken up by clouds and rained out. The oxidation of these compounds is significantly slower than might be expected based on the atmospheric composition of 20% molecular oxygen (O_2). The inefficiency of ground state O_2 as an atmospheric oxidant is due to its electronic structure. With two unpaired electrons it is a spin-triplet (total spin quantum number S=1, giving a term symbol of $^3\Sigma_g^-$). In

Atmospheric
Chemistry
and Physics
Discussions

32   contrast, virtually all trace chemicals emitted into the atmosphere contain only paired

33   electrons and are thus spin-singlets (S=0). From a simplistic perspective (i.e. ignoring

34   nuclear spin interactions, inter-system crossings, nuclear dipole effects etc.) the spin

35   selection rule, $\Delta S=0$, means that the reaction of ground state O_2 with most emitted

36   compounds is effectively spin forbidden. Electronically excited O_2 ($^1\Delta_g$ or $^1\Sigma_g^+$) is a

37   spin singlet and is more reactive in the atmosphere but low concentrations limit its

38   role [*Larson and Marley*, 1999]. Instead, atmospheric oxidation proceeds

39   predominantly via reactions with spin-doublet oxygen-derived species (S=½), notably

40   the hydroxyl (OH) and peroxy radicals ($RO_2 = HO_2$, CH_3O_2, $C_2H_5O_2$, etc.), or spin-

41   singlet species (e.g. ozone (O_3)).

42   One of the few spin-triplet species in the atmosphere other than O_2 is the ground state

43   of atomic oxygen ($O(^3P)$), which readily undergoes a spin allowed reaction with O_2 to

44   produce the spin-singlet O_3 molecule. This spin allowed reaction is responsible for the

45   creation of O_3 in both the stratosphere, where it forms the protective O_3 layer, and the

46   troposphere. The ability of O_3 to oxidise other spin-singlet species makes it a powerful

47   oxidant, and it is thus considered a pollutant with negative health effects. Sources of

48    $O(^3P)$ within the troposphere are limited because solar photons at sufficiently short

49   wavelengths to directly photolyse O_2 to $O(^3P)$ are essentially unavailable.

50   Aside from the photolysis of O_3 itself, the only other significant source of

51   tropospheric $O(^3P)$ is the photolysis of nitrogen dioxide (NO_2) [*Crutzen*, 1971].

52   Nitrogen oxides are emitted into the troposphere as nitrogen oxide (NO), which can be

53   oxidised to NO_2 by O_3 and other oxidants. A large thermodynamic energy barrier

54   prevents oxidation of NO to NO_2 by the OH radical [*Nguyen et al.*, 1998], and

55   therefore NO oxidation occurs through reaction with either O_3 or RO_2. In terms of O_3

56   production, the oxidation of NO by O_3 forms a null cycle. Thus only the reaction of

57   NO with RO_2 leads to a net production of O_3.

58   Exploring the distribution, source and sinks of tropospheric O_3 is a central theme of

59   atmospheric science. Chemical transport models (online and offline) are essential

60   tools enabling this understanding but their validity needs to be continually assessed.

61   Model-model comparison exercises are commonly performed to assess performance,

62   and comparisons of modelled O_3 budgets traditionally form part of this assessment

63   [*Stevenson et al.*, 2006; *Wu et al.*, 2007; *Wild*, 2007; *Young et al.*, 2013]. Ozone

64   production is diagnosed from the flux of NO to NO_2 via reaction with each of the

Atmospheric
Chemistry
and Physics
Discussions

65 speciated RO_2 in the model's chemical schemes. This approach provides information

66 on the relative importance of the different RO_2 in the fast $NO + RO_2$ reactions within

67 the model, but gives very little detail on how the longer time scale model processes

68 (emissions, chemistry, deposition) influence O_3 production. Thus exploring the

69 reasons that models differ in their O_3 production is difficult and progress has been

70 slow.

71 A new diagnostic framework that links large scale model drivers such as emission,

72 chemistry, and deposition to O_3 production would allow an improved assessment of

73 why model ozone budgets differ. We attempt to provide such a framework here.

74 2. A new diagnostic framework.

75 The rate of production of tropospheric O_3 is limited by the rate of oxidation of NO to

76 NO_2, which is in turn limited by the rate of production of peroxy radicals (RO_2).

77 Peroxy radicals form through association reactions of hydrogen (H) atoms or alkyl

78 radicals (both spin-doublets, $S=\frac{1}{2}$) with O_2, forming a highly reactive spin-doublet

79 radical on an oxygen atom. This spin allowed reaction converts spin-triplet O_2 that

80 cannot react with spin-singlet pollutants into a spin-doublet O_2 containing species that

81 can. As such the formation of RO_2 is central to the atmosphere's oxidation capacity,

82 and its production is limited by the rate of production of H atoms or alkyl radicals.

83 Thus the maximum potential rate of tropospheric O_3 production is equal to the rate at

84 which H atoms and alkyl radicals are produced.

85 Hydrogen atoms and alkyl radicals are predominantly produced via the spin allowed

86 breaking of the spin-pairing between the two electrons in a C or H containing covalent

87 bond ($S=0$), such as those in hydrocarbons. These spin-pairings can be broken in the

88 atmosphere either chemically or photolytically, with the products necessarily

89 conserving spin. The breaking of a covalent bond by a photon ($s=1$) can result in two

90 products with $S=\frac{1}{2}$ or two products with $S=0$. Likewise, oxidation by a radical ($S = \frac{1}{2}$)

91 will result in one product with $S=0$ and one with $S=\frac{1}{2}$, because the unpaired electron

92 on the radical reactant pairs with one of the covalent bond electrons to produce a spin-

93 singlet.

94 Although the majority of RO_2 is formed from emitted C or H containing covalent

95 bonds, there are a few notable exceptions. Hydrogen atoms can also be produced

96 through the oxidation of CO to CO_2 by OH. During this reaction the coordinate bond

Atmospheric
Chemistry
and Physics
Discussions

97   between the C and O atom is broken and the H atom is produced via the breaking of

98   the O-H bond. The other notable exception is the oxidation of an SO_2 lone pair of

99   electrons to SO_3 by OH, where again the H atom produced comes from the OH. In

100   both of these exceptions a spin-singlet electron pairing (CO coordinate bond or SO_2

101   lone pair) is broken during the production of the H atom, and we can therefore

102   consider these reactions as similar to the breaking of C or H containing covalent bond.

103   For simplicity these spin-singlet electron pairings that can be broken in the

104   troposphere to produce either a H atom or alkyl radical will be referred to as

105   "oxidisable bonds" (C-C, C-H, C=C, CO coordinate bond, S:).

106   Tropospheric O_3 production occurs through the oxidation of NO by RO_2. Following

107   the above rationale, these RO_2 are produced during the spin allowed breaking of

108   oxidisable bonds predominantly contained within emitted VOCs. This perspective

109   allows us to build a new metric for the production of tropospheric O_3 based around the

110   spin conserving properties of oxidisable bond breaking. In the extreme case, all

111   oxidisable bonds are photolysed to produce two spin-doublet RO_2 products, which

112   then react exclusively with NO to generate O_3. Thus at steady state, the maximum rate

113   of O_3 production is equal to the rate of production of RO_2, which is equal to twice the

114   rate of destruction of the number of oxidisable bonds. This in turn is equal to twice the

115   rate of emission of oxidisable bonds. Deviation from this maximum is determined by:

116   • The relative importance of processes that produce spin-singlet vs. spin-
117   doublet products during oxidisable bond breaking;

118   • The fraction of spin-doublet products from oxidisable bond breaking which
119   form RO_2;

120   • The fraction of RO_2 that go on to oxidize NO to NO_2.

121   To illustrate this Fig. 1 shows the tropospheric oxidation of a methane (CH_4) molecule

122   through various steps to either a carbon dioxide (CO_2) molecule or a species that is

123   deposited (CH_3OOH, CH_2O, CH_3NO_3). Methane contains 4 x C-H oxidisable bonds

124   (8 paired bonding-electrons) and as the oxidation proceeds, the number of oxidisable

125   bonds decays to zero. Figure 1 highlights the steps in the tropospheric CH_4 oxidation

126   mechanism that form spin-doublet products, with between 1 and 5 RO_2 produced

127   depending on the oxidation pathway. This compares with the theoretical maximum of

128   8 if all the original C-H bonds were photolysed to yield 2 spin-doublet products.

Atmospheric
Chemistry
and Physics
Discussions
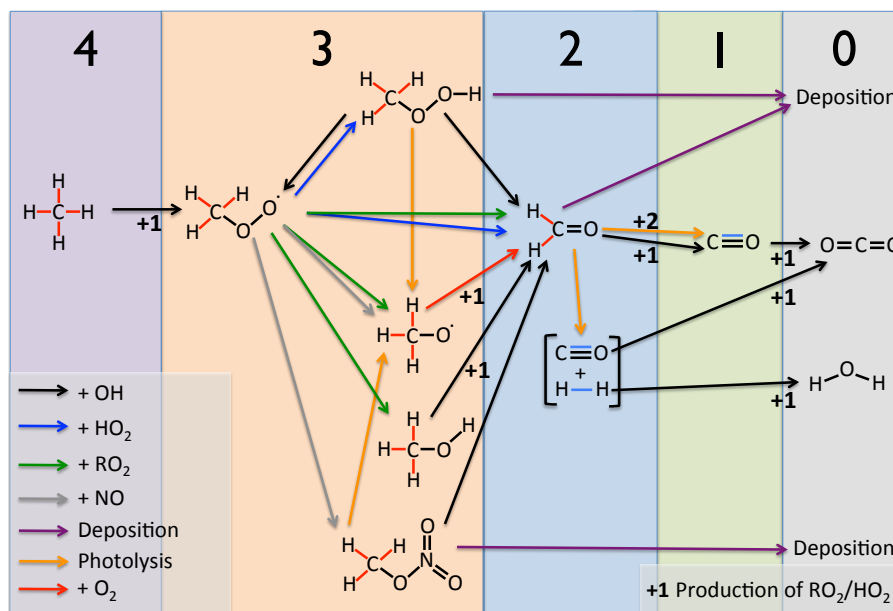
129

130 **Figure 1. Peroxy radical production during the tropospheric oxidation of CH₄.**

131 **Moving from left to right, the oxidisable bonds (emitted = red, produced = blue)**

132 **present in CH₄ are removed via a range of tropospheric processes, indicated by**

133 **the coloured arrows. The large numbers across top of the figure indicate the**

134 **number of oxidisable bonds at each stage of this oxidation. The production of**

135 **RO₂ is indicated by the +1/+2 numbers with the associated process arrows for**

136 **producing 1 or 2 RO₂ respectively.**

137 The principal atmospheric source of oxidisable bonds is the emission of C-H, C-C and

138 C=C bonds in hydrocarbons, with the only other significant sources being the

139 emission of CO and the chemical production of CO and H_2 during hydrocarbon

140 oxidation. Over a long enough timescale, the global atmosphere can be considered to

141 be in a chemical steady state, where the rate of loss of oxidisable bonds is balanced by

142 the rate of production or emission. Thus the O_3 production rate can be described by

143 equation (1), where the O_3 production metric P_sO_3 is equal to the number of spin-

144 paired electrons in oxidisable bonds (i.e. twice the sum of the number of oxidisable

145 bonds emitted (E_{bonds}) and chemically produced (P_{bonds})), multiplied by the number of

146 spin-doublet radicals produced per oxidisable bond break divided by the maximum of

147 2 ($F_{Radicals}$), multiplied by the fraction of the radicals produced which are RO_2 (F_{RO2}),

148 multiplied by the fraction of RO_2 that goes on to react with an NO to produce an O_3

149   molecule (F_{NO}). A small correction (I) for the production of RO_2 via reactions of spin-

150   doublet radicals other than those that result in the breaking of oxidisable spin-pairings

151   (e.g. $O_3 + OH \rightarrow HO_2 + O_2$) is included.

152    $$P_sO_3 = \left(\left(2 \times (E_{bonds} + P_{bonds}) \times F_{radicals} \times F_{RO_2} \right) + I \right) \times F_{NO} \qquad (1)$$

3. Implementation

154   We use the GEOS-Chem model to evaluate this new O_3 production diagnostic. GEOS-

155   Chem is a global chemical transport model of tropospheric chemistry, aerosol and

156   transport (www.geos-chem.org version 9-02). The model is forced by assimilated

157   meteorological and surface fields (GEOS-5) from NASA's Global Modelling and

158   Assimilation Office, and was run at 4°x5° spatial resolution. The model chemistry

159   scheme includes O_X, HO_X, NO_X, BrO_X and VOC chemistry as described in Mao et al.

160   [2013] as are the emissions. The new P_sO_3 diagnostic has been implemented via the

161   tracking of reactions by type in the GEOS-Chem chemical mechanism file (further

162   details given in the SI). This tracking of reactions enables the fate of all oxidisable

163   bonds as well as the production and loss of all RO_2 within the model to be determined

164   using the standard GEOS-Chem production and loss diagnostic tools. Model

165   simulations were run for 2 years (July 1st 2005 – July 1st 2007) with the first year used

166   as a spin up and the diagnostics performed on the second year.

167   The standard GEOS-Chem diagnostic for O_3 production (PO_3) is shown on the left

168   side of Table 1. This emphasizes the very fast cycling between NO and NO_2, but

169   provides little in terms of higher process level information. The right side of Table 1

170   shows the new budget for P_sO_3, which tracks the processing of oxidisable bonds

171   within the model. Both diagnostic methods give the same final answer but our new

172   methodology provides more process level detail. Figure 2 illustrates this new process

173   based approach, showing the flow of emitted oxidisable spin-paired electrons (bonds)

174   to O_3 and the magnitude of the various mechanisms that contribute to and compete

175   with O_3 production. The annual oxidisable bond emission of 389 T mol yr^{-1} has the

176   potential to create 778 T mol yr^{-1} of radicals. If all oxidisable bonds were broken by

177   photons to produce two radical products the RO_2 production would be 778 T mol yr^{-1}.

178   If the oxidisable bonds were instead broken via radical reaction (e.g. OH) then RO_2

179   production would be 389 T mol yr^{-1}. The various oxidisable bond breaking / removal

Atmospheric
Chemistry
and Physics
Discussions

Open Access

180   pathways within the model result in the production of 280 T mol yr^{-1} of RO_2, with the

181   remainder largely producing stable spin singlet products.

182   Of the 280 T mol yr^{-1} RO_2 produced, 112 T mol yr^{-1} reacts with NO to produce O_3.

183   The remainder is lost through the reaction or deposition of RO_2 reservoir species

184   (RO_{2y} = RO_2 + peroxides + peroxy-acetyl nitrates). For example the production of

185   methylperoxide (CH_3O_2 + HO_2 = CH_3OOH) results in the loss of 2 RO_2's. However,

186   the reaction of methylperoxide with OH can re-release CH_3O_2 (CH_3OOH + OH =

187   CH_3O_2 + H_2O). Thus, the production of methylperoxide represents the loss of a HO_2

188   and the movement of a CH_3O_2 into a peroxide RO_{2y} reservoir species. The deposition

189   of a peroxide molecule is thus the loss of a RO_{2y} reservoir species. Notable in Fig. 2 is

190   that the role of PAN and nitrate removal of global RO_{2y} is negligible, instead being

191   dominated by peroxide production and loss and the reaction of RO_2 with O_3.

PO_3 / T mol Yr^{-1}		PO_3 / T mol Yr^{-1} (except $F_{Radicals}$, F_{RO2}, and F_{NO} which are all unitless)	
NO + HO_2 → NO_2	74	E_{bonds}	330
NO + CH_3O_2 → NO_2	27	P_{bonds}	58
Other RO_2 + NO → NO_2	10	$F_{radicals}$	0.40
Other	1	F_{RO2}	0.86
		Inorganic RO_2 source	15
		F_{NO}	0.40
PO_3	112	P_sO_3	112

192   **Table 1. Comparison of ozone production diagnostics for GEOS-Chem base**

193   **simulation. Standard model PO$_3$ diagnostics (left column) show reactions**

194   **responsible for NO to NO$_2$ conversions but provide little process level**

195   **information. The new P$_s$O$_3$ (right) provides increased information on the**

196   **processes controlling O$_3$ production within the model.**

Atmospheric
Chemistry
and Physics
Discussions
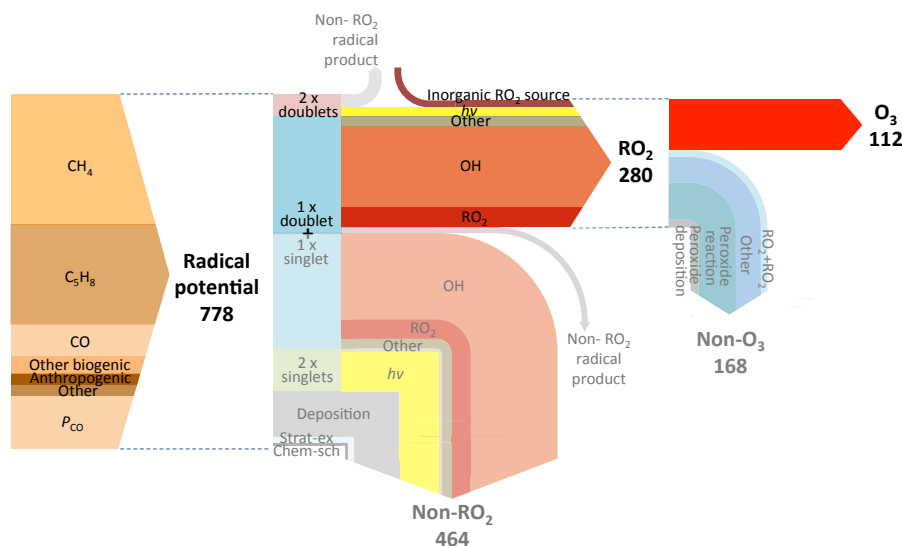
197
198 **Figure 2. Flow of oxidisable bonds to O$_3$ production in the GEOS-Chem base**
199 **simulation. Arrows are coloured according to process and the arrow thickness is**
200 **proportional to the flux through that channel. Spin-paired electrons are input as**
201 **oxidisable bonds into the model (left arrow), with the potential to create 778 T**
202 **mol yr^{-1} of radicals. The actual fate of these bonds is shown in the central arrow,**
203 **producing 280 T mol yr^{-1} of RO$_2$, of which 112 T mol yr^{-1} reacts with NO to**
204 **produce O$_3$ (right arrow).**

3.1 Emitted oxidisable bonds

206 The fuel for tropospheric oxidation chemistry is the emission of oxidisable bonds,
207 predominantly in the form of hydrocarbons. The production of tropospheric O$_3$ from
208 the spin-paired bonding electrons emitted into the standard GEOS-Chem model
209 occurs with an efficiency of 14% (112 T mol yr^{-1} molecules of O$_3$ produced / 778 T
210 mol yr^{-1} spin-paired electrons emitted as oxidisable bonds, Fig.2). These spin-paired
211 bonding electrons are predominantly emitted in the form of CH$_4$, isoprene (C$_5$H$_8$) and
212 CO (37%, 28%, and 9% respectively). Oxidisable bonds produced during chemical
213 reactions (P$_{bonds}$), account for 15% of the net source. Figure 3 shows emissions of CO
214 and hydrocarbons in the standard GEOS-Chem simulation in terms of mass of carbon
215 per compound, number of oxidisable bonds per compound and as number of bonds in
216 different oxidisable bond types. The commonly used carbon mass approach splits
217 emissions approximately equally between each of the major sources (CH$_4$ (29%),

218   Isoprene (32%) and CO (30%)). In contrast, the oxidisable bonds accounting approach

219   apportions hydrocarbon emissions 44%, 33% and 11% for CH_4, isoprene and CO

220   respectively. This highlights the high number of oxidisable bonds per carbon atom in

221   CH_4 (4) compared to isoprene (2.8) and CO (1). Thus efforts to consider emissions on

222   a per-bond basis may provide more insight into chemical processes, as it is these

223   bonds that ultimately determine the chain-like chemistry rather than the mass of

224   carbon atoms. This helps to emphasise the relative importance of CH_4 emissions on

225   global tropospheric chemistry compared with other emissions such as isoprene or CO.

226   The type of oxidisable bond emitted is overwhelmingly C-H (71%).
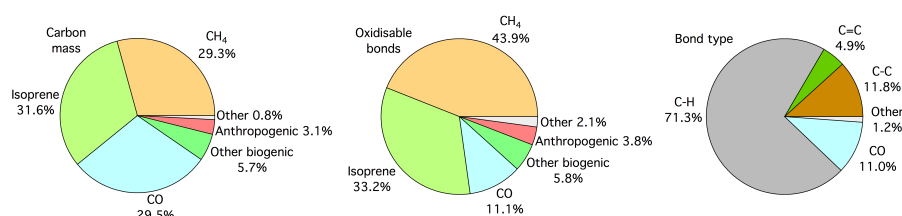
227
228   **Figure 3. Pie charts showing hydrocarbon emissions in the base GEOS-Chem**

229   **simulation. Emissions split by carbon mass (left), number of oxidisable bonds**

230   **(centre) and bond type (right).**

231   The total emission and production of oxidisable bonds has the potential to create 778

232   T mol yr^{-1} of radicals. However, only 6% of the oxidisable spin-pairings are broken to

233   give the maximum 2 spin-doublet products (e.g. radical channel of CH_2O photolysis).

234   The majority (68%) are oxidized via reaction with a spin-doublet species (OH) to

235   produce 1 spin-singlet and 1 spin-doublet product (e.g. OH + VOC). The remaining

236   26% of spin-paired electrons are removed to form two spin-singlets (e.g. the non-

237   radical channel of CH_2O photolysis). Thus, of the 778 Tmol yr^{-1} spin-paired electrons

238   emitted or produced only 265 T mol yr^{-1} (34%) are converted into RO_2, with an

239   additional 15 T mol yr^{-1} produced from reactions such as $O_3 + OH \rightarrow HO_2 + O_2$ (*I*).

240   The efficiency of O_3 production from the available oxidisable bonds is further reduced

241   as only 40% of the 280 T mol yr^{-1} of RO_2 produced react with NO to produce NO_2.

242   The remainder is lost either through the self-reaction of RO_2 or via loss through

243   deposition or reaction of RO_{2y} reservoir species (e.g. peroxides). Thus overall 14% of

244   the emitted bonding electrons go on to make O_3.

245   This new O_3 production diagnostic shows the impact of processes such as emission,

246   deposition and chemical mechanism, providing significantly more detail than the

247   standard PO_3 diagnostic approach (Table 1). We now explore the sensitivity of model

248   O_3 production to changing emissions of NO_x and VOC from the perspective of the

249   two diagnostic methods.

4 Model sensitivities

251   Understanding model response to changing emissions is an important tool for

252   considering policy interventions. The major controls on O_3 production are emissions

253   of NO_x and VOCs. We show in Fig. 2 that from the perspective of global O_3

254   production, oxidisable bond emissions are dominated by CH_4 and isoprene. Figure 4

255   shows the impact of changing emissions of NO_x, isoprene and CH_4 on O_3 production

256   from both the perspective of this new methodology and the conventional $NO+RO_2$

257   diagnostic approach. The following sections investigate these model responses and

258   use the new diagnostic to provide insight into the processes driving the observed

259   response in O_3 production.

260

261

Atmospheric
Chemistry
and Physics
Discussions
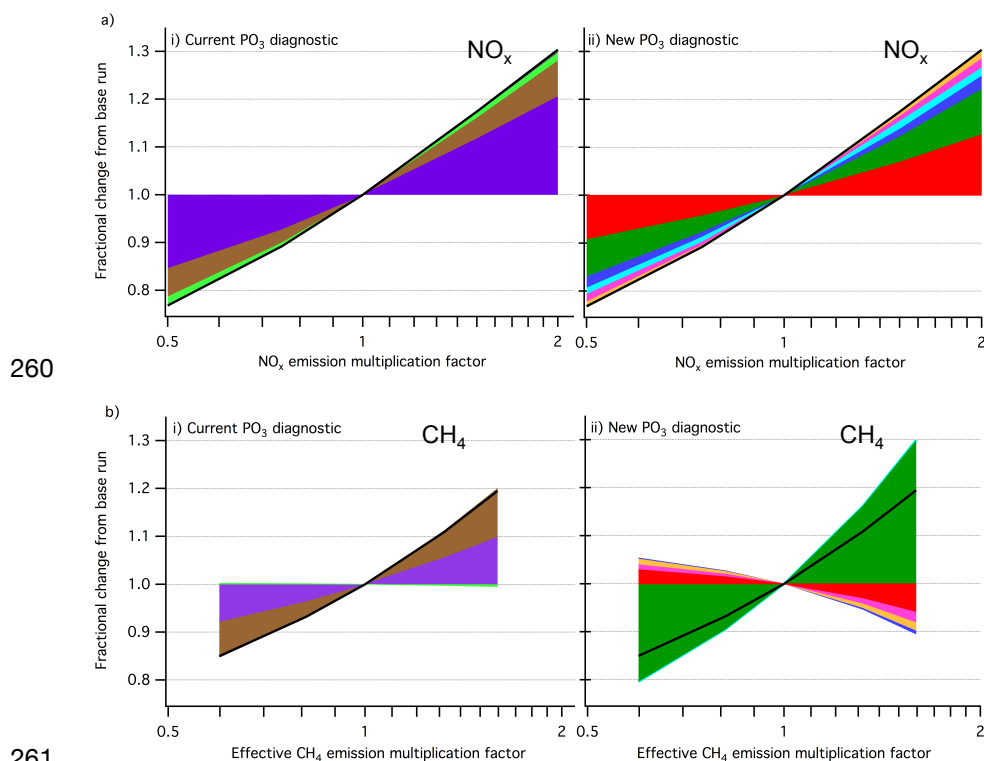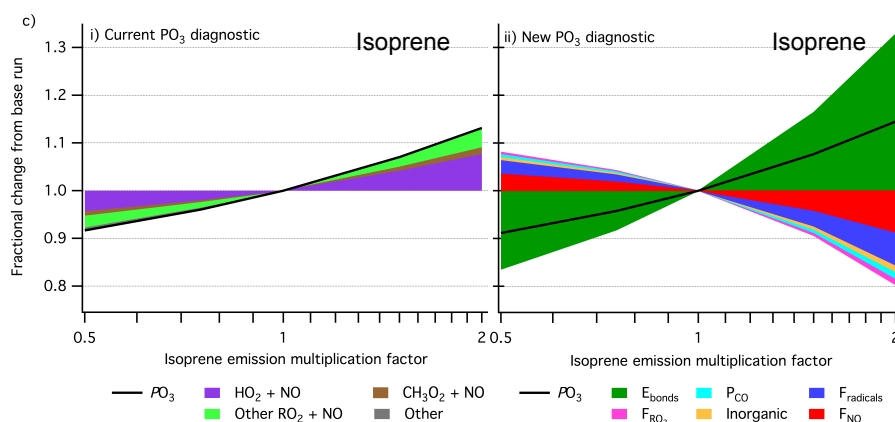
Figure 4. Understanding the effect of NO_x and VOC emissions on ozone production at the process level. Stack plots showing fractional change in model PO_3 compared to base simulation and associated contributions from the current PO_3 (i) and new P_sO_3 (ii) diagnostic parameters under changing NO_x emissions (a), effective CH_4 emission (b) and isoprene emission (c).
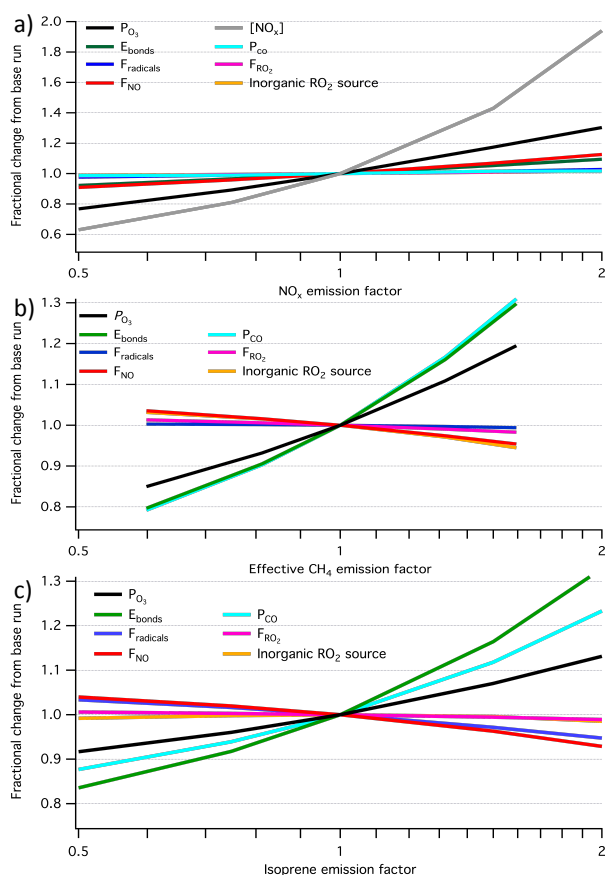
4.1 NO_x emissions

Figure 4a diagnoses the relative response of GEOS-Chem O_3 production to changing NO_x emissions, using simulations where NO_x emissions from anthropogenic, biomass burning, biofuels, soil and lighting sources were multiplied by factors of 0.5 - 2. Increasing NO_x emissions increases O_3 production. The standard RO_2+NO diagnostic (Fig.4a(i)) shows that fractional contributions to the total change in PO_3 from HO_2 (67%), methyl-peroxy (MO_2) (25%), and other RO_2 (8%) remain approximately constant across the NO_x emission range investigated. This diagnostic provides little detail on the processes driving the change in O_3 production under changing NO_x emissions. In contrast, Fig. 4a(ii) is based on the new P_sO_3 diagnostic and shows a range of process level changes occurring as NO_x emissions change.

4.1.1 Impact of changing NO_x emission on F_{NO}

Unsurprisingly, as NO_x emissions increase the fraction of RO_2 reacting with NO to produce NO_2 (F_{NO}) increases (red section in Fig. 4a(ii)). However, this impact only accounts for around 40% of the increase in P_sO_3. Figure 5a shows the fractional change in all the P_sO_3 efficiency parameters and the global mean NO_x concentration as a function of the changing NO_x emission. As NO_x emissions increase the increase

285   in NO_x concentration in the model is somewhat dampened. Halving the NO_x emission

286   leads to NO_x burdens dropping by ~35%, and doubling leads to an increase of 95%.

287   This dampening is due to the impact of NO_x emissions on OH (see section 4.1.2),

288   which is the dominant sink for NO_x. Increasing NO_x increases OH concentrations,

289   which in turn shortens the NO_x lifetime thus dampening the response of concentration

290   to emission.

291

Figure 5. Fractional change in new P_sO_3 diagnostic parameters from base run

against changing NO_x emission (a); effective CH_4 emission (b); and isoprene

emission (c).

295   The response of F_{NO} to changes in NO_x emissions is also dampened relative to the

296   change in NO_x emissions. This is due to spatial variability in F_{NO}, which is not

297   affected uniformly by changing NO_x emissions. Figure 6 shows the probability

Atmospheric
Chemistry
and Physics
Discussions

298   distribution of F_{NO} values across all model grid boxes for the base simulation and the

299   half and doubled NO_x emission simulations (black, blue and red lines respectively).

300   For example, in a grid-box in the continental boundary layer where RO_2 reacts

301   overwhelmingly with NO, doubling the NO_x emission may move F_{NO} from 0.90 to

302   0.95 but it can't double it. Similarly, in the remote boundary layer where RO_2 reacts

303   overwhelmingly with other RO_2 doubling NO_x emissions may move F_{NO} from 0.3 to

304   0.4 but again it doesn't double. Thus the geographical spread of NO_x chemistry limits

305   the change in F_{NO} caused by changing NO_x emissions. The spatial variability in the

306   new P_sO_3 diagnostic parameters shows that this approach has significant potential in

307   the analysis of regional O_3 budgets as well as global.
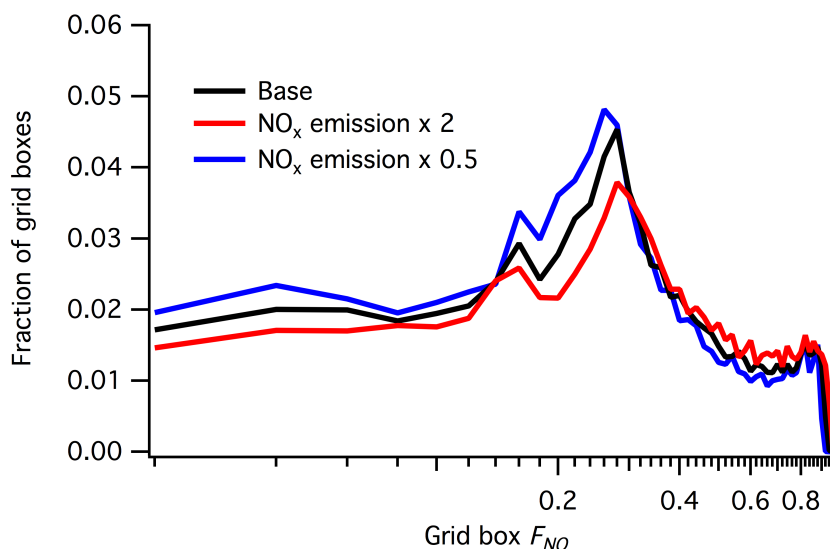
308

309   **Figure 6. Effect of NO_x emission on distribution of F_{NO} values (log scale). F_{NO}**

310   **values for each model grid box in the base and NO_x emission x 0.5 and x 2**

311   **simulations, split into 50 x 0.02 width bins.**

312   **4.1.2 Impact of changing NO_x emission on E_{bonds}**

313   Figure 4a(ii) shows that 60% of the response in P_sO_3 to changing NO_x emission is due

314   to factors other than F_{NO}, with 40% of the increase due to changes in the emissions

315   (E_{bonds}: 32%) and chemical production (P_{bonds}: 8%) of oxidizable bonds. This increase

316   in E_{bonds} is surprising given VOC emissions are unchanged in these simulations.

317   However, increasing NO_x emissions results in an increased OH concentration in the

Atmospheric
Chemistry
and Physics
Discussions

318 model, which then leads to an increase in CH_4 oxidation. GEOS-Chem fixes CH_4

319 concentrations resulting in an increase in the effective CH_4 emissions as OH

320 concentrations increase, causing an increase in the total bond emission (E_{bonds}). Figure

321 7 shows the response of model global mean OH concentration and effective CH_4 bond

322 emission as a function of global mean NO_x concentration across the simulations where

323 the base NO_x emissions are multiplied by factors from 0.5 to 2. More CH_4 oxidation

324 also leads to more CH_2O production and in turn more CO production (P_{CO}),

325 accounting for a significant fraction of the increase in this term.
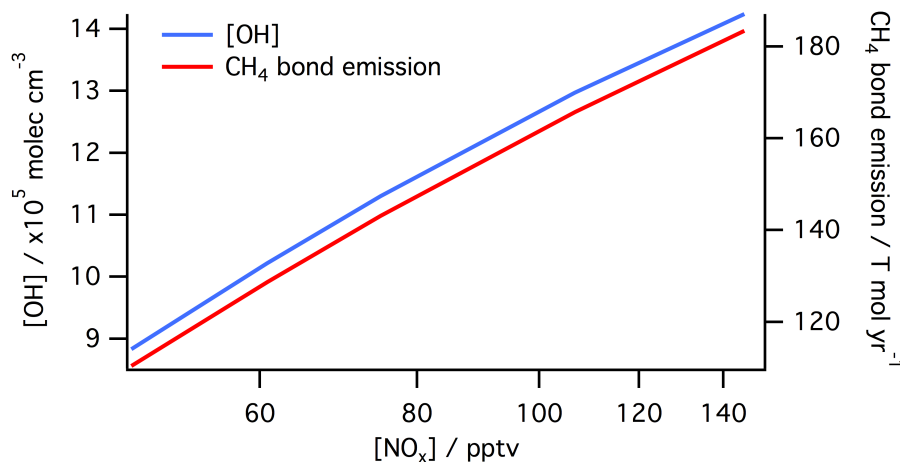
326

327 **Figure 7. Global mean OH concentration and effective CH_4 emission as a**

328 **function of [NO_x]. Plot shows effective CH_4 emission tracks OH concentration in**

329 **simulations where the NO_x emission was increased or decreased from the base**

330 **simulation. Note X-axis log scale.**

331 **4.1.3 Impact of changing NO_x emission on $F_{radicals}$, F_{RO2} and I**

332 The fraction of radicals produced from bond oxidation ($F_{radicals}$) and the fraction of

333 those radicals which are RO_2 (F_{RO2}) show slight positive increase with NO_x emission,

334 accounting for 9% and 6% of the change in P_sO_3 respectively. This reflects changes in

335 the partitioning of the fate of the oxidisable bonds, and is largely due to the changes in

336 OH. As OH increases with NO_x emission, the rate of chemical oxidation of bonds

337 increases at the expense of other losses, in particular deposition. The inorganic RO_2

338 source term (I) also correlates with NO_x emission, as it is largely determined by the

339   concentrations of OH and O_3. This change accounts for 5% of the observed change in

340   P_sO_3.

341   Thus, with this new diagnostic methodology it is evident that only 40% of the model

342   O_3 production response to changing NO_x emission is due to the direct effect of

343   increasing NO concentration on the rate of $RO_2 + NO$ reactions. Another 40% is due

344   to fixing the concentration of CH_4 within the model, with the final 20% due to the

345   increased OH competing for the available oxidisable bonds.

346   **4.2 Changing effective CH_4 emissions**

347   Figure 4b shows the effect on the O_3 production diagnostic of varying the prescribed

348   CH_4 concentrations by factors of between 0.5 and 2 from the base simulation. The

349   CH_4 emission rate (plotted) is diagnosed from the loss rate of CH_4 to reaction with

350   OH, the only CH_4 loss in the model. We describe this as the effective CH_4 emission.

351   As effective CH_4 emission increases, O_3 production also increases. The standard

352   diagnostic (Fig.4b(i)) shows that this increase occurs through an increased rate of

353   reaction of HO_2 and CH_3O_2 with NO, as would be expected as these are the RO_2

354   produced during CH_4 oxidation. The rate of other $RO_2 + NO$ reactions actually

355   decreases slightly as CH_4 emissions increase, due to lower OH concentrations and

356   increased competition for NO from HO_2 and CH_3O_2. The new diagnostic (Fig.4b(ii)),

357   however, shows the increase in O_3 production with increasing effective CH_4 emission

358   is not simply a result of more HO_2 and MO_2.

359   **4.2.1 Impact of changing effective CH_4 emission on F_{NO}**

360   The observed change in P_sO_3 is around one third smaller than would be expected from

361   the increase in the oxidisable bond emission (E_{bonds}) and bond production (P_{bonds})

362   terms alone. This is due to a countering decrease in the other efficiency parameters

363   with increasing effective CH_4 emission. Figure 5b shows the fractional change in all

364   the efficiency parameters as a function of the changing effective CH_4 emission. The

365   decrease in the fraction of RO_2 reacting with NO to produce NO_2 (F_{NO}) is driven by

366   increasing O_3 concentrations, which push the NO/NO_2 ratio towards NO_2. This

367   reduces the availability of NO to react with RO_2 thereby reducing O_3 production. This

368   shift in the NO/NO_2 ratio also increases NO_x loss within the model with increasing

369   CH_4 emission, as the increased CH_4 oxidation increases RO_2 concentrations resulting

Atmospheric
Chemistry
and Physics
Discussions

370 in larger losses of NO$_2$ via compounds such as peroxyacetyl nitrate (PAN) and

371 peroxynitric acid (PNA).

4.2.2 Impact of changing effective CH$_4$ emission on E$_{bonds}$

373 As CH$_4$ is the largest single source of oxidisable bonds (Fig. 3), increasing the

374 effective CH$_4$ emission results in an increase in E$_{bonds}$. Changing the fraction of total

375 emitted oxidisable bonds from CH$_4$ does however have significant consequences on

376 the loss mechanisms of these bonds, which influences the other efficiency parameters.

377 The pie charts in Fig. 8 show the split of oxidisable bond loss mechanisms in the base

378 simulation and those with the CH$_4$ concentration fields multiplied by 0.5 and 2. As the

379 effective CH$_4$ emission increases the fraction of bonds lost via OH decreases, despite

380 the actual number of oxidisable bonds lost to OH increasing. A larger fraction of

381 bonds are therefore lost via the other mechanisms shown in Fig. 8 rather than reaction

382 with OH. As CH$_4$ removal occurs predominantly in the free troposphere, increasing

383 the effective CH$_4$ emission also results in a reduction in the fraction of oxidisable

384 bonds lost via deposition. The largest fractional increase in bond loss mechanism with

385 increasing effective CH$_4$ emission is for photolysis, with the increase in the "other"

386 fraction due to increased loss of bonds to the stratosphere with increasing CH$_4$. The

387 fraction of bonds lost via other chemistry (e.g. non-OH radical oxidation and RO$_2$ self

388 reactions) remains approximately constant across the effective CH$_4$ emission scenarios

389 investigated.
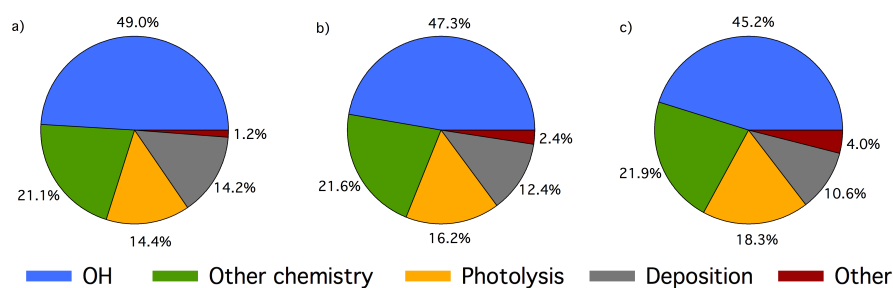
Figure 8. Oxidisable bond loss mechanisms under changing CH$_4$ emissions. Pie charts showing fractional loss mechanisms for oxidisable bonds in model simulations with 0.5 x CH$_4$ concentration field (a), base simulation (b) and 2 x CH$_4$ concentration field.

4.2.3 Impact of changing effective CH_4 emission on $F_{radicals}$, F_{RO2} and I

The fraction of oxidisable bonds that goes on to produce radicals ($F_{radicals}$) and the fraction of these that are RO_2 (F_{RO2}) also decrease with increasing effective CH_4 emissions. This is due to decreasing global OH concentration resulting from increased loss by reaction with CH_4 and a decreasing NO concentration. This favours bond loss via pathways such as deposition rather than those that produce RO_2. These changes are predominantly due to the chemistry of CH_2O. As shown in Fig. 1, the oxidation of CH_2O occurs either via reaction with OH or photolysis, with OH reaction yielding 1 RO_2 from the net breaking of 2 spin-singlet bonds, and the two photolysis channels yielding either 0 x RO_2 (spin-singlet products molecular channel) or 2 x RO_2 (spin-doublet products radical channel), with the molecular channel being dominant. The reduction in OH concentration with increasing CH_4 means photolysis increases its competition as a bond loss mechanism, which has the effect of reducing the average RO_2 production per CH_2O oxidised. The increase in the fraction of total bonds lost through the CH_2O photolysis as CH_4 increases thus results in a reduction in both $F_{radicals}$ and F_{RO2}. The reduction in $F_{radicals}$ due to changing CH_2O fate, however, is largely offset by a reduction in the fraction of bonds lost via deposition as CH_4 increases. This is due to the long lifetime of CH_4 compared with the majority of other sources of oxidisable bonds, resulting in oxidation increasing fractionally in the free troposphere where deposition is a less significant loss mechanism than in the boundary layer.

4.3 Changing isoprene emission

The species through which the oxidisable bonds are emitted has a significant impact on O_3 production, due to their subsequent removal mechanisms. For example, in a simulation where the only emission of oxidisable bonds is CO, $F_{radicals}$ is 0.5 and F_{RO2} is 1 as the only CO sink is reaction with OH to produce one HO_2 (OH + CO → HO_2 + CO_2). The CO coordinate bond, which in theory has the potential to produce 2 radicals, only produces 1 radical, which is an RO_2.

Isoprene has the most complex chemistry in the model and is the second largest source of bonds into the atmosphere (Fig. 3). Figure 4c shows the response of the two O_3 production diagnostics to varying the isoprene emission within the model. The standard diagnostic (Fig.4c(i)) shows that the most significant increase in PO_3 from

427   increasing isoprene emissions is from $NO + HO_2$ and non-MO_2 peroxy radicals, with a

428   smaller increase from MO_2. The new P_sO_3 diagnostic (Fig.4c(ii)) again provides more

429   insight, showing significant offsetting of around a half between the terms.

430   **4.3.1 Impact of changing isoprene emission on F_{NO}**

431   The increased isoprene emission leads to a similar change in the magnitude of the

432   total number of oxidisable bonds emitted (E_{bonds}) as the simulations in which effective

433   CH_4 emission were varied. However, the countering decrease in all of the efficiency

434   parameters is much larger for isoprene than for CH_4. Figure 5c shows the fractional

435   change in the new P_sO_3 ozone production diagnostic parameters as a function of

436   isoprene emissions compared to the base simulation. The change in F_{NO} is due to both

437   a decrease in global mean NO_x concentrations with increasing isoprene and the spatial

438   distribution of isoprene emissions. With the majority of global isoprene emissions

439   being in regions with low NO_x emissions, and thus low values of F_{NO}. Figure 9 shows

440   a decrease in global mean NO_x, and global mean OH, concentrations with increasing

441   isoprene emissions, however, the effect is less than that seen when CH_4 is responsible

442   for the same increase in oxidisable bond emission. This is due in a large part to the

443   spatial scales over which the two compounds impact.
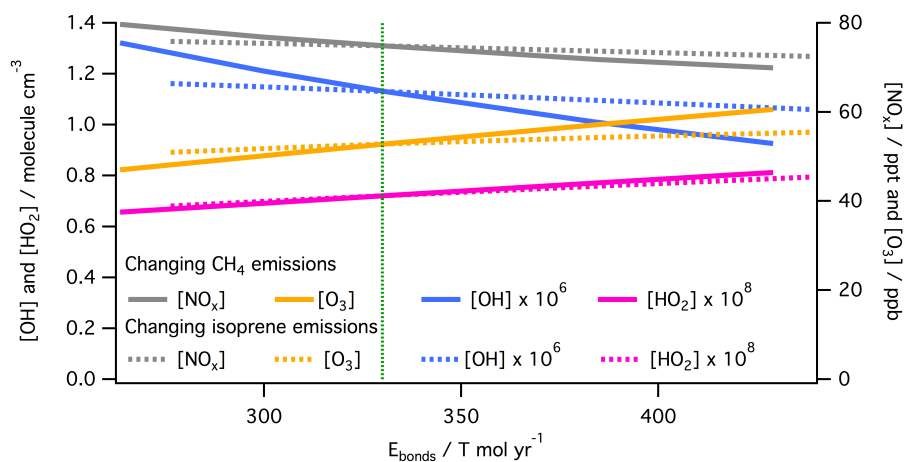

444

445   **Figure 9. The effect of oxidisable bond parent species on OH, HO₂, O₃ and NO$_x$**

446   **concentrations. Global mean [OH], [HO₂], [O₃] and [NO$_x$] for simulations where**

447   **the effective CH₄ emission (solid lines) and isoprene emission (dashed lines) were**

448   **changed, against model E$_{bonds}$. The dashed vertical green line indicates E$_{bonds}$ in**

449   **the base simulation (330 T mol yr^{-1}).**

Atmospheric
Chemistry
and Physics
Discussions

450 **4.2.2 Impact of changing isoprene emission on E_{bonds}**

451 As isoprene is the second largest source of oxidisable bonds (Fig. 3), increasing the

452 isoprene emission results in a significant increase in E_{bonds}. Differences in both the

453 spatial distribution of emissions and the oxidation chemistry of isoprene and CH_4,

454 however, means that the impact of the increases in E_{bonds} on O_3 production are

455 significantly different for the two compounds. This is predominantly because the

456 fraction of oxidisable bonds that are physically deposited for isoprene is high

457 compared to those emitted as CH_4. This increase is due to i) the higher solubility of

458 isoprene oxidation products compared to those of CH_4, and ii) the higher reactivity of

459 isoprene means its oxidation occurs in the boundary layer where both dry and wet

460 deposition is most effective.

461 Figure 10 shows the split of oxidisable bond loss mechanisms in the base simulation

462 and those with the isoprene emissions multiplied by 0.5 and 2. The complex myriad of

463 products formed during the isoprene oxidation mechanism also results in the

464 production of many highly oxygenated multifunctional compounds with high Henrys

465 law solubility constants, meaning they are more readily lost to deposition.
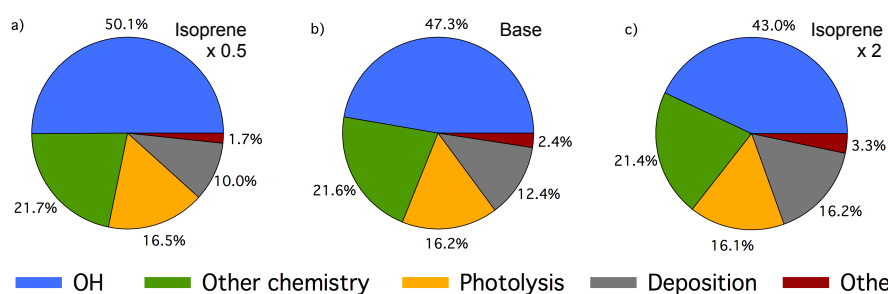
466
OH ▪ Other chemistry ▪ Photolysis ▪ Deposition ▪ Other

467 **Figure 10. Oxidisable bond loss mechanisms under changing isoprene emissions.**

468 **Pie charts showing fractional loss mechanisms for oxidisable bonds in model**

469 **simulations with 0.5 x isoprene emission (a), base simulation (b) and 2 x isoprene**

470 **emission (c).**

471 Increasing the isoprene emission also has a slight offsetting impact on the effective

472 CH_4 emission, as increased isoprene concentrations decrease OH concentrations, and

473 thus decrease the effective CH_4 emission. A doubling in isoprene emission causes a

474 6% reduction in the effective emission of CH_4.

475

Atmospheric
Chemistry
and Physics
Discussions

476   **4.3.3 Impact of changing isoprene emission on $F_{radicals}$, F_{RO2} and I**

477   As shown in Fig. 3c(ii), increasing the isoprene emission results in a reduction in all

478   P_sO_3 efficiency parameters. The reductions in $F_{radicals}$ is due to the higher fraction of

479   oxidisable bonds that are lost via non-radical forming pathways (e.g. deposition) for

480   isoprene relative to the other main oxidisable bond emission sources CH_4 and CO.

481   The slight decreases of F_{RO2} and I with increasing isoprene emission are

482   predominantly due to changes in OH and NO_x (Fig. 9).

483   The complex chemistry of isoprene oxidation combined with the spatial distribution of

484   isoprene emissions means the increase in O_3 production due to increases in isoprene

485   emissions is roughly half what might be expected from the increase in oxidisable bond

486   emission alone (i.e. if the increase was *via* CO instead of isoprene).

487   # 5. Conclusions

488   We have shown that this bond-focussed approach to O_3 production provides a

489   significantly more detailed understanding of the processes involved. The role of

490   modelled VOC emissions and O_3 burden has been reported previously [*Wild*, 2007;

491   *Young et al.*, 2013]. However previous efforts extending this to a general process led

492   approach has not been successful. This new approach provides a tool with which the

493   processes controlling O_3 production can be investigated, and a metric by which

494   different emissions can be compared. For example, the differing chemistry of isoprene

495   and CH_4 shows that even though their emissions of carbon mass are comparable, the

496   atmosphere responds in different ways, with the isoprene bonds being less effective in

497   producing O_3 than CH_4 bonds. By quantifying multiple steps in the O_3 production

498   process, competing changes in the system become apparent (as shown in Fig. 4b(ii)

499   and c(ii)) and are thus testable. This enables the effect of model approximations on O_3

500   production to be quantified (e.g. the effect of NO_x on CH_4 emissions when using CH_4

501   concentration fields).

502   This new diagnostic also points towards the importance of observational datasets for

503   assessing our understanding of tropospheric chemistry. Although the budget presented

504   in Fig. 2 provides an annually integrated global estimate it points towards local

505   comparisons that can be made to assess model fidelity. Comparisons, both their

506   magnitude and their ratios, between observed and modelled bond concentration, bond

507   emission and loss fluxes (e.g. OH reactivity [*Yang et al.*, 2016] or depositional fluxes

Atmospheric
Chemistry
and Physics
Discussions

Open Access

508   [*Wesely and Hicks*, 2000]), and O_3 production [*Cazorla and Brune*, 2010] would all

509   provide comparisons for outputs from the P_sO_3 diagnostic and help assess model

510   performance.

511   Another potentially important application is in model-model comparisons. Increases

512   in our understanding of why different models calculate different O_3 production and

513   burdens has been slow [*Stevenson et al.*, 2006; *Wu et al.*, 2007; *Young et al.*, 2013]. A

514   comparison between models based on this methodology may well help identify at a

515   process level why models differ in their O_3 production.   The application of this

516   diagnostic to regional O_3 production should also increase insight into the processes

517   controlling model O_3.

Atmospheric
Chemistry
and Physics
Discussions

References

Cazorla, M., and W. H. Brune (2010), Measurement of ozone production sensor, *Atmos. Meas. Tech.*, *3*(3), 545–555, doi:10.5194/amt-3-545-2010.

Crutzen, P. J. (1971), Ozone production rates in an oxygen-hydrogen-nitrogen oxide atmosphere, *J. Geophys. Res.*, *76*(30), 7311–7327, doi:10.1029/JC076i030p07311.

Kroll, J. H. et al. (2011), Carbon oxidation state as a metric for describing the chemistry of atmospheric organic aerosol., *Nat. Chem.*, *3*(2), 133–139, doi:10.1038/nchem.948.

Larson, R. A., and K. A. Marley (1999), Singlet oxygen in the environment, *Environ. Photochem.*, *2*, 123–136.

Levy, H. (1973), Photochemistry of minor constituents in the troposphere, *Planet. Space Sci.*, *21*(4), 575–591, doi:10.1016/0032-0633(73)90071-8.

Mao, J., F. Paulot, D. J. Jacob, R. C. Cohen, J. D. Crounse, P. O. Wennberg, C. A. Keller, R. C. Hudman, M. P. Barkley, and L. W. Horowitz (2013), Ozone and organic nitrates over the eastern United States: Sensitivity to isoprene chemistry, *J. Geophys. Res. Atmos.*, *118*(19), 1–13, doi:10.1002/jgrd.50817.

Nguyen, M. T., R. Sumathi, D. Sengupta, and J. Peeters (1998), Theoretical analysis of reactions related to the HNO2 energy surface: OH + NO and H + NO2, *Chem. Phys.*, *230*(1), 1–11, doi:10.1016/S0301-0104(97)00383-2.

Stevenson, D. S. et al. (2006), Multimodel ensemble simulations of present-day and near-future tropospheric ozone, *J. Geophys. Res. Atmos.*, *111*(8), doi:10.1029/2005JD006338.

Wesely, M. L., and B. B. Hicks (2000), A review of the current status of knowledge on dry deposition, , *34*.

Wild, O. (2007), Modelling the global tropospheric ozone budget: exploring the variability in current models, *Atmos. Chem. Phys.*, *7*, 2643–2660, doi:10.5194/acpd-7-1995-2007.

Wu, S., L. J. Mickley, D. J. Jacob, J. A. Logan, R. M. Yantosca, and D. Rind (2007), Why are there large differences between models in global budgets of

Atmospheric
Chemistry
and Physics
Discussions

548   tropospheric ozone?, *J. Geophys. Res. Atmos.*, *112*(5), 1–18,
549   doi:10.1029/2006JD007801.

550 Yang, Y., M. Shao, X. Wang, A. C. Nölscher, S. Kessel, A. Guenther, and J. Williams
551   (2016), Towards a quantitative understanding of total OH reactivity: A review,
552   *Atmos. Environ.*, *134*(2), doi:10.1016/j.atmosenv.2016.03.010.

553 Young, P. J. et al. (2013), Pre-industrial to end 21st century projections of
554   tropospheric ozone from the Atmospheric Chemistry and Climate Model
555   Biogeosciences Intercomparison Project (ACCMIP), *Atmos. Chem. Phys.*,
556   *13*(10), 5277–5298, doi:10.5194/acp-13-5277-2013.

557

Author contributions

559 All work presented here was conceived by P.M.E. and M.J.E. The implementation,
560 model simulations and analysis were carried out by P.M.E., and the manuscript was
561 written by P.M.E. with substantial input from M.J.E..

Additional information

563 The authors declare no competing financial interests.

Acknowledgements